

DATA SCIENCE AND IOT MANAGEMENT SYSTEM

ISSN: 3068-272X www.ijdim.com Original Research Paper

HDL BASED DESIGN FOR 32 BIT RIPPLE CARRY ADDER FOR DIGITAL DESIGN

Mistry Surindrakour Avatarsingh¹, Dr. M. Pavithra Jyothi²

¹PG Scholar, Department of VLSI System Design, Shadan Women's College of Engineering and Technology, sonamkarabin@gmail.com

²Assoc Professor, Department of ECE, Shadan Women's College of Engineering and Technology

Received: 02-08-2025 Accepted: 04-09-2025 Published: 11-09-2025

ABSTRACT

The ripple carry adder (RCA) is the most basic method for implementing a summing operation in CMOS-based electronics. A half-adder, which is perhaps the most basic integration circuit, was recently proposed by the scientific discipline, which studies data processing via spin waves and the quanta magnons. To facilitate the design and Modeling of gates and circuits of any complexity, we provide a computation model for the basic blocks. We illustrate its operation using a 32-bit basic RCA as an example. It is demonstrated that to equalize the magnon frequencies between the half-adders, the RCA necessitates the use of extra regenerators based on direction couplers with integrated amplifiers. Electronic circuits on a big scale are benchmarked. When considering all necessary amplifiers as well as the electrical power usage of a 30 nm-based 32-bit adder can be as modest as 961 per execution.

1. INTRODUCTION

Because of their prospective uses as carriers of data in upcoming information processing innovations, spinning waves (SWs) especially their quantamagnons—have garnered a lot of attention in recent years. A rigid the body's spinning order is disturbed by spin waves, which happen when there is no electron transport and, thus, no heating by joule. Furthermore, the wave's characteristics (destructive disturbances, diffraction, etc.) simplifies the design of the framework for wave-based gated logic, and the spin wave's time offers extra angles of flexibility (beyond loudness) to code knowledge. Additionally, the GHz to THz frequency band has a nanotechnology a wavelength that is only constrained downwards by the attraction material's lattice structure constant. Additionally, the stated and versatile unpredictable spin-wave phenomenon are distinct from sound waves and magnetic microwaves that are microwave thereby making them offering for both RF technology and Boolean algebra and unconventional (such as neuromorphic) the field of computing. circuits can beat CMOS-based devices by up to 10 times in terms of energy usage, according to evaluations of the first incorporated circuit, which was presented in the form of a half adder. The footprint of a 30-nm-based half adder is like that of a 7-nm-based CMOS half adder; however, it takes 18 ns to process data instead of CMOS having a clock velocity of 3 GHz, 0.3 ns. It is anticipated that the newly released inverse-design s would significantly improve all the attributes by at least one order of magnitude. However, rather than being positioned in engineering or production, s is still predominantly in the academic physics realm. Even with its rapid growth, there are still several challenges to be solved. The biggest problem, as covered in this book, is the requirement for extremely effective lowenergy transistors with powerful integrators to

transform the spinning waves into electrically generated signals. Numerous equipment, such as preponderance gates, spin wave logic gates, and magnon semiconductors, have previously been shown at the early stage of individual logic gate that level. There are two primary methods for building circuits. The first is known as "converter-based" and is based on the employment of extremely effective magnon-tocurrent converters that are employed following each data transfer. This method's foundational devices were initially presented and explained in. Furthermore, the important problems of standardization and fan out were resolved. The alternative method, known as "allmagnon," uses naturally occurring, highly prominent regressive events to minimize the translator number, even if some translation from magnon to current remains necessary. The asymmetric operation of a no unidirectional coupler was demonstrated successfully. Additionally, it was demonstrated statistically that integrating two couplers with directional characteristics into a circuit can result in the realization of a half-adder, which consists of an AND logic barrier and an XOR logic gate that operates simultaneously. With the addition of a low-energy amplifiers, the half-adder was specifically made to be suitable for additional integration. However, because these types of simulations are numerically extremely costly and impractical, the circuitry that would enable the simultaneous functioning of several these gadgets together to accomplish complicated arithmetic operations was well outside the purview of the earlier studies. In fact, it becomes difficult to complete realistic simulations in an acceptable length of time as the total number of elements increases. That method's excellent precision comes with substantial computational expenses and can take a long time to achieve. Because of these factors, tiny models are



DATA SCIENCE AND IOT MANAGEMENT SYSTEM

ISSN: 3068-272X www.ijdim.com **Original Research Paper**

essential for investigating new technologies, and traditional CMOS technology use the same methodology. Compact models are essential for developing electronic circuits and operate as a conduit for information exchange between designers of circuits and technologists/physicists. Here, we offer an algebraic framework that enables the construction of intricate all-magnon networks using the functional building blocks of the half-adder that was previously examined.

PROPOSED METHOD

The ripple carrying addition is the simplest combinations of circuits to utilize when implementing a summing. The mathematical logic units and other processing components in many computers' designs employ adders. The full adder (FA) is the core component of such an adder. N-bit variables can be added by cascading many complete adders in sequence. In this approach, the carry-out bit ripples into the following step, as its name implies. Three of the inputs (Ai, Bi, and Ci-1) are added by the complete adder, which also generates two outputs (Si, Ci+1), which stand for what was added and the carryout, separately.

2. LITERATURE SURVEY

1. The phase changes in spin wave energy caused by wall domains

We investigate the interplay between magnetism boundary walls and spin waves, two crucial characteristics of ferrous nanostructures. Magneto static spin waves are believed to undergo phase changes when they travel through domain barriers, according to microscopic calculations. We propose to investigate this impact by dividing the waves on several ring branches, much like in an A haronov - B ohm experiment. The domain barriers in the branches determine how merging waves interfere. The initial step approaching nanoscale magnetized devices carrying out logical processes based on spin-wave propagation may be the carefully monitored manipulation of spin-wave stages.

2. A quantitative investigation of the configuration of the signal analyser in a spin-wave storage computer

This work uses spin waves created in a Ferrous magnet zirconia layer to statistically investigate the effects of signal detection configuration on reserve computing speed. This study is fundamentally significant because, as the spin waves travel in the film in a geographically dispersed way, they not only transmit the data that was supplied but also change it into multidimensional communication space. A rich reservoir-computational functionality is realized by these stochastic dynamics. To get the geographic distribution of the storage tank

modes that respond to given input information, which can be modelled as spin vectors and utilized for a neural network's waveform classification problem, we first recreate spin waves in a hexagonal garnets film that has two input terminals. A result is produced by combining the displayed weights of connections with the observed reservoir statuses. After training, we arrange the output neurons at square points, equilateral circle points, or randomly to see the values' location in space and talk about their numbers and locations. By varying the number of output electrodes and we assess how well classification works and discover that, independent of grid, circular, or arbitrarily configuration, a high accuracy (> 90%) can be obtained with just a few tens of output poles. These findings imply that the dynamics of the spin waves are rich and complicated enough for this kind of work. Then, by positioning the electrodes locally on the chip, we examine which region has a greater distribution of pertinent data. Lastly, we demonstrate the device's capacity to generalize for input wavesignal frequencies within a particular frequency spectrum. Soon, these findings will enable the development of spin-wave repository technologies enabling inexpensively sophisticated computer.

3. Connected half-added numbers using a unidirectional connection

logical gates, transistors, however, and subunits for non-Boolean computation are examples of parts of devices that have previously been constructed. Magnons, the quanta that are part of spin waves, might be utilized to encode data in beyond-Moore computations. Although they can serve as building blocks for circuits, directed couplers are also being studied but have proven unfeasible due to their multi-mode spectrum and millimetre size. Here we present a directional coupler based on 350 nm wide single-mode waves in waveguides made of iridium. iron silicate. According to the signal strength, number, and applied field of magnets, we utilize a spin-wave's intensity to encode data and direct it to one of the coupler's two outputs. We also suggest an integrated half-adder with two couplers in each direction which processes all data in the magnon domain while using the least amount of energy possible using micro magneto Modeling.

4. Electromagnetic signalling using spin-wave translation in a magnetized isolator

An insulator's energy spectrum gap is sufficiently wide to stop conduction of electricity and particle excitement. However, an electron contains spin along with to charge, and in some insulation materials, the group mobility on spin can spread and transmit a signal. Magnetic waves are typically employed to stimulate this acceleration, which is known as a spin wave. Here, we demonstrate how spins-Hall effects, which allow electricity to be



DATA SCIENCE AND IOT MANAGEMENT SYSTEM

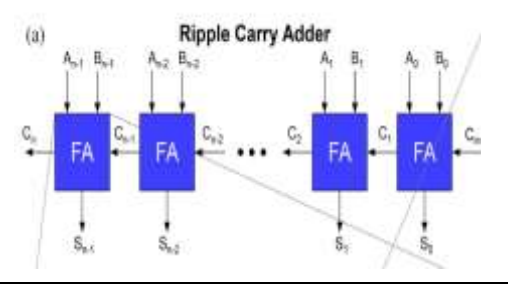
ISSN: 3068-272X www.ijdim.com Original Research Paper

directly converted into a spin wave and then transmitted through (and recovered from) a semiconductor over substantial boundaries, can be used to create and measure a spin extend in an absorber. First, we demonstrate that a platinum layer and an insulator magnet Y3Fe5O12 may transmit spin acceleration. Through spin-Hall effects4-11, this transfer enables the immediate transformation of an electrical current in the palladium coating to a spin pulse in the Y3Fe5O12. Furthermore, we show that an electric current in one metal film produces voltage in the other, far-off, metal film by using the mechanism of transfer in a Pt/Y3Fe5O12/Pt system. In particular, the spun-Hall influence in the beginning platinum itself film transforms the supplied electrical charge into spin kinetic energy, which is then transported by a spin wave in the insulating Y3Fe5O12 layer. At the next platinum itself film, the direction of spin velocity the spin wave's velocity is transformed back into a voltage that is electric. A magnetic field may be used to turn this effect on and off. Y3Fe5O12's openness for the conveyance of spin acceleration is caused by little spin damping. Improved signal conveyance in electrical systems and devices may be possible with this blended power transmission technique.

5. A thin hydrogen iron diamond film with a threeport logic gates employing upstream volume spin waves interaction

We present a logic gate that uses the disruption of forwarding volumetric spin waves (FVSWs) moving through an yttrium iron granite bandwidth that is 100µm wide and 54 nm thick. The waveguide is produced epitaxially on a garnet substrate. By altering their phase difference, two FVSWs injected by coplanar waveguides were able to interfere both productively and systematically, displaying an XNOR logic activity. Spin wave collectors were used to attenuate the reflections and harmonic waves produced at the waveguide's edges. When a strong magnetic field of around 2.80kOe (=223kAm-1) was applied horizontally to the material, the measured seclusion ratio was 19dB. The device's length was around 53 µm, and its wavelength was approximately 8.9µm. Additionally, threedimensional in form radio wave calculations were used to analyse the entanglement status of the SWs.

3. PROPOSED METHODOLOGY 3.1 BLOCK DIAGRAM



3.2 PART EXPLAINATION: OPERATIONAL RULE REGARDING ADDER CONSTRUCTION

The ripple-based carry addition is the simplest circuit type to utilize when implementing a summing. The computational logic unit and other processors components in many computing designs employ adders. The full adder (FA) is the essential component of such an adder. N-bit variables can be added by cascading many complete addition algorithms in parallel. In this approach, the complete bit ripples into the following step, as its name implies.

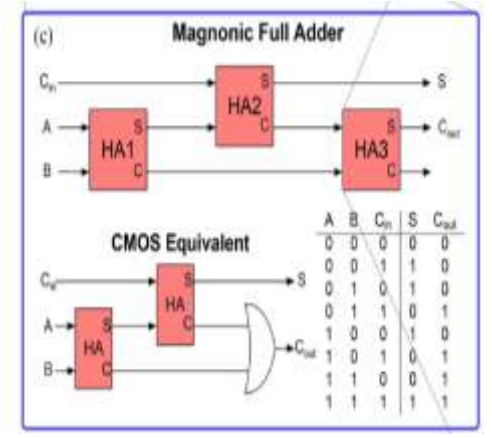
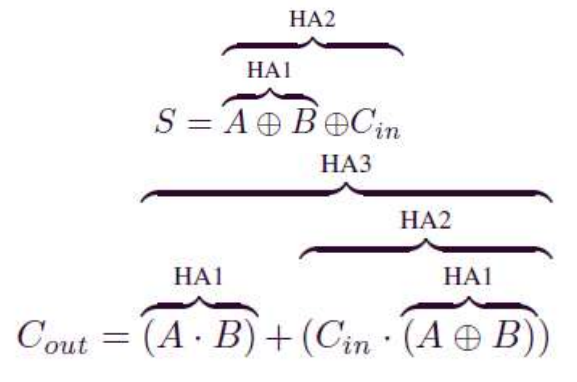


Figure 3.1 shows the Drift Transport Adder functional component diagram.

Three inputs (Ai, Bi, and Ci-1) are added by the complete adder, which also generates a couple of outcomes (Si, Ci+1), which stand for the sum along with the carry-out, respectfully. There are several methods for executing it; Figure provides an instance. Based on the partial adder (HA), the most crucial fundamental component for logic computing, the architecture shown in Figure 1(b) was created. Specifically, three adder rings are used in the design suggested in this work. The over parenthesis indicates the operation carried out by each HA, and the carriedout logic functionality is provided in (1) and (2) for the aggregate and carrier, separately.



It is evident from Figure 1 (c) that the final HA is solely utilized as an OR gate. Figure 1(c) reports the CMOS counterpart and its truth table for the sake of clarity. The two couplers with directions (DCs) that



DATA SCIENCE AND IOT MANAGEMENT SYSTEM

ISSN: 3068-272X www.ijdim.com Original Research Paper

make up the half of the adder are DC1 and DC2, correspondingly; one operates in the nonlinear domain and the other is used in the non-stationary regime (Figure 1(b)). As shown in both diagrams in Figure 1(b), dipolar interaction between perpendicular wavelength guides causes a dispersion curve to break into balanced (s) and anti-symmetric forms (as) in both situations. Ms = 1.4×105 Am-1, exchange stiffness $A = 3.5 \times 10-12 J/m$, and a few additional geometrical factors have been taken into consideration while obtaining the diffusion interactions:

 $Lw2 = 3\mu m$, d2 = 210 nm, $\phi2 = 20^{\circ}$, $\sigma2 = 10$ nm, Lw1=370 nm, d1 =450 nm, ϕ 1 =20 \circ , σ 1 =50 nm. Each mode can be stimulated concurrently in the connected wave paths when the stimulated spin wave is higher than the antisymmetric mode's lowest (f = 2.282 GHzin Figure 1(b)). Despite having the same the rate, the two types' wave numbers (k s and k as) vary, which causes a distinct phase accumulation. The dipolar linked wavelength guides transmit energy because of these two modes interfering with one another. Coupling length Lc is the term for the sequential energy transfer generated by spin wave components in one resonator and both. Figure 1(e) shows a schematic representation of this phenomenon, which is calculable as:

$$L_c = \frac{\pi}{\Delta k_x} = \frac{\pi}{|k_s - k_{as}|}$$

Numerous factors, including the rotational wave's strength, wavelength of light, and waveguide's geometry parameter for affect the relationship's length [32]– [34]. In the linear regime, the DC1 functions as a power splitter, while in the non-linear domain, the DC2 functions as a while/XOR gate. The standardized output power in the linked Guides is as a proportion of the connection length Lc is displayed as illustrated in Figure 1(d). They can be used to express it.

$$\frac{P_{1out}}{P_{1out} + P_{2out}} = \cos^2\left(\frac{\pi L_w}{2L_c}\right),$$

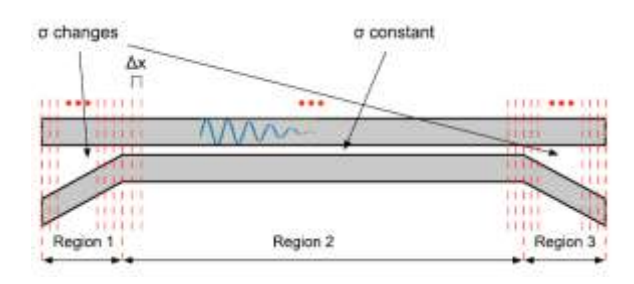
where the width of the connected area is denoted by Lw. According to the standardized output power speech, power splits and the operation of the couplers that are directional are significantly influenced by the length of the linked area and the relationship length. It should be noted that while we suppose a spin wave having the appropriate amplitude enters the adder under study from separate unit, we do not consider a device that differentiates combining electrical in nature and outputs in this research. The "all-magnon strategy" assumes that the conversion operation is only necessary twice—once at the input and once at the output of the complete chip—and that efficiency in conversion is not a major factor. Therefore, spin waves may be excited and detected using any of the existing methods.

DESIGN OF PORTABLE PHYSICOCHEMICAL

Solving the Landau-Lifshitz equations for the motion of magnetized is the most precise method for determining the ratio of dispersion of two connected waveguides. Nevertheless, this method is too intricate and operationally costly to incorporate into a circuitlevel research tool. The given small physiological model, on the different hand, maintains a high level of precision and offers the freedom to investigate circuits considering their physical characteristics. On the Git hub computing/spin shout model, it is publicly accessible. The scattering connection of the DC1 and DC2 is described by the model we created, which is dependent on the spin wave amplitude and the geometry of the couplers. It considers the irregular width distribution of the waveguide's basic spin wave type as well as damper inefficiencies. As the effect of anchoring diminishes, the waveguide's functional width (Weff) may exceed its nominal width (w). A shift in the dispersion curve causes the coupling length Lc to vary, which in turn causes a changing output power partition. It gives the equation for calculating the scattered relation between two connected waveguides.

$$f_{a,as}^{nl}(k_x, a_k) = f_{s,as}^0(k_x) + T_k|a_k|^2,$$

where Tk is the regressive change in frequency coefficients in the isolated waveguide, ak is a without dimensions variable which reflects the magnitude of the spin wave its magnitude, and f0s, as(kx) is the scattering relation for the symmetric antisymmetric spun waves patterns in connected Guides are over the linear area. The key components of pathways with three primary areas are the unidirectional couplers. area 2 displays the linked area where the wave paths are parallel to one another, whereas Countries 1 and 3 depict each of the oblique branching (opening/closing arms). Most of the energy transmission between the linked waveguides is seen in area 2, where the DC1 and DC2 (100 nm technology node) have very tiny gaps (σ) of 50 nm and 10 nm, respectively. Nevertheless, regions 1 and 3 also contribute in some way. The number of leaps along the connected area 2 may be defined as N = Lw/Lc using the power partition formula presented in. The calculation may be rewritten as $\cos 2 \pi 2$ N by replacing in. The ensuing negative and positive interference determine the length of hops from one microwave to the other.





DATA SCIENCE AND IOT MANAGEMENT SYSTEM

ISSN: 3068-272X www.ijdim.com

Original Research Paper

Figure 2. Three areas may be distinguished in the unidirectional coupler: region 2 exhibits a constant separation among the two waveguides, whereas regions 1 and 3 display a varying distance. Region 2 contributes the most to the distribution curve. The opening/closing arms (regions 1 and 3) create an extra connection that may be taken into consideration thanks to the discretization process that is applied along the x axis.

All the energy is transmitted to the other channel whenever the two phases' phase separation is 180° $(\Delta \phi = \pi)$. Thus, given an overall phase building up of πN , the mode can execute several leaps equivalent to N along the connected area. It may therefore be translated as:

$$\frac{P_{1out}}{P_{1out} + P_{2out}} = cos^2 \bigg(\frac{\Delta \varphi}{2}\bigg)$$

The beginning of the scatter curve and the nonzero oscillation coefficient, which are reliant on the spin wave strength inside the directed coupler, determine the relationship length Lc. The spin wave strength is not continuous along the propagation direction if the waveguide under consideration is not optimal but has losses. In the actual situation, the spin pulse frequency decays exponentially with increasing propagated distance: e(-|2x|/x freepath), where x represents range and xfreepath, which may be computed using formula 4 in, represents decline length, is also insufficient as it only considers a fixed bonding length, but the spacedependent spin wave power causes Lc to fluctuate continually throughout the waveguide. The average coupling length (La, avg) is introduced in the revised formula in accordance with

$$L_{a,avg} = \frac{\pi L_w}{\Delta \varphi}$$

Combining the waveform quantity fluctuation across the route of propagation direction Δφ=|ks-kas|dx yields the phase accumulating among the two modes. The unidirectional modulator in the simulation is broken across the x-axis with a step size of Δx for a total of M. The stage change $\Delta \phi$ may thus be calculated as follows:

$$\Delta \varphi = \sum_{i=1}^{M} \Delta k_i \Delta x$$

The distinction among the two wave indices is computed at every subinterval i. The model also considers the connection that the opening and closing arms produce. Regions 1 and 3 are therefore dismissed, albeit the difference varies in this case. The unshifted dispersal relationship, which is dependent on the gap σ , is where the computation begins for those locations. The average coupling length and, thus, the power that output divided may be accurately estimated thanks to the persistent phase accretion.

METHOD OF SIMULATION **Connection of scattering**

Two technologies nodes—the 100 nm and the 30 nm—are considered in the mathematical framework that was created. The guide width is represented by the node. For hydrogen iron gemstone (YIG), we considered a few additional parameters such as: interchange stiffness $A = 3.5 \times 10-12 \text{Jm}-1$, absorption $\alpha = 2 \times 10-4$, and magnification saturation $Ms = 1.4 \times 105 Am - 1$. Although YIG was selected due to its minimal spin-wave damping, the idea created here ought to work with any other attraction substance. Based on the work in, the dispersion connection of the spin extend mode in an enclosed resonator is represented as.

$$f_0(k_x) = \frac{1}{2\pi} \{\Omega^{yy}\Omega^{zz}\}^{1/2}$$

 $= \frac{1}{2\pi} \{ (\omega_H + \omega_M(\lambda^2 k_x^2 + F_{k_x}^{yy}(0))) \}$
 $(\omega_H + \omega_M(\lambda^2 k_x^2 + F_{k_x}^{zz}(0))) \}^{1/2}$

Where:

$$\Omega^{ii} = \omega_H + \omega_M (\lambda^2 k_x^2 + F_{k_x}^{ii}(0)), i=y, z.$$
 $\omega_H = \gamma B_{ext}, \gamma$ is the gyro magnetic ratio, and B ext is external magnetic field.

 $\omega M = \gamma Ms$, Ms is the saturation magnetization.

$$\lambda = \sqrt{2 A/(\mu_0 M_s^2)}$$
 Is the exchange length, A is the exchange stiffness, and $\mu 0$ is permeability of vacuum.

For kinetic magneto dipolar in the F conversations, the term kx Be leg Giaetal created the tensor `F kx formula. can be computed by applying the Fourier-space method:

$$\hat{F}_{k_x}(d) = \frac{1}{2\pi} \int_{-t}^{+t} \hat{N}_k e^{ik_y d} dk_y$$

$$\hat{N}_{k} = \frac{|\sigma_{k}|^{2}}{\widetilde{w}} \begin{pmatrix} \frac{k_{x}^{2}}{k^{2}} f(kh) & \frac{k_{x}k_{y}}{k^{2}} f(kh) & 0 \\ \frac{k_{x}k_{y}}{k^{2}} f(kh) & \frac{k_{y}^{2}}{k^{2}} f(kh) & 0 \\ 0 & 0 & 1 - f(kh) \end{pmatrix}$$

$$\sigma_k = 2 \frac{k_y \cos\left(\frac{\kappa w}{2}\right) \sin\left(\frac{k_y w}{2}\right) - \kappa \cos\left(\frac{k_y w}{2}\right) \sin\left(\frac{\kappa w}{2}\right)}{k_y^2 - \kappa^2}$$

$$\widetilde{w} = \frac{w}{2} \left(1 + \operatorname{sinc}\left(\kappa w\right)\right)$$



DATA SCIENCE AND IOT MANAGEMENT SYSTEM

ISSN: 3068-272X www.ijdim.com Original Research Paper

$$f(kh) = 1 - \frac{1 - e^{-kh}}{kh}$$
$$k = \sqrt{k_x^2 + k_y^2}$$

Additionally, h is the channel width, which for the 100 Angstroms and 30 nm innovation nodes is 30 nanometre and 10 nm, accordingly.

When d = 0, the self-dipolar attraction is represented by the tensor Fkx (d); when calculated at separation d, the dipole relationship among the waveguides is represented by the tensor Fkx (d). The integral restriction 1 = 10 and d = 0 apply to the solitary microwave. Keep in mind that 1 may be infinite in the best scenario. Nonetheless, this integral's primary effects are located around l = 0. The diffusion relation of two connected waves in waveguides may be obtained starting from these concepts. It is possible to calculate the split among the asymmetrical and anti-symmetric modes based on the divalent connection.

$$f_{s,as}(k_x) = \frac{1}{2\pi} \sqrt{(\Omega^{yy} \pm \omega_M F^{yy}_{kx}(d))(\Omega^{zz} \pm \omega_M F^{zz}_{kx}(d))}$$

$$\Omega^{ii} = \omega_H + \omega_M (\lambda^2 k_x^2 + F_{k_x}^{ii}(0)), i=y, z.$$

 $d = w + \delta$, where w is the waveguide's width and δ is the distance from one wavelength to the other. It is used to compute fiikx(d).

The spin pulse profile in connected Guides are differs slightly from that in solo waveguides. The (16) was unable to explain for the disparity, though. Reducing the integral constraint of is one way to correct for this issue.at our instance, the integral restriction is lowered from 10 to 0.53 for DC1 and 0.63DC2 at the 100 nm technologies node. In this instance, there is good agreement between the computed and replicated dispersion curves. This suggests that the spin extend profile is not significantly altered by a little adjustment in the gap. It is feasible to determine the related wave number and calculate the signal migrating in large circuits by using the dispersion equation calculated for isolated and connected waveguides.

Geometry: The accepted technological node has a strong relationship with the practical morphologies of the directional couplers shown in Figure 1(b). The primary geometrical variables for the DC1 for the 100 nm YIG are Lw1 = 370 nm, d1 = 450 nm, $\phi 1 = 20^{\circ}$, and $\sigma 1 = 50$ nm. The subsequent characteristics form the basis of the DC2: $d2 = 210 \text{ nm}, \ \phi 2 = 20^{\circ}, \ \sigma 2 = 10$ nm, and Lw2 = 3 μ m. Lw1 = 230 nm, d1 = 50 nm, ϕ 1 $= 20^{\circ}$, $\sigma 1 = 20$ nm, Lw2 = 2460 μ m, d2 = 70 nm, $\phi 2 =$ 20° , $\sigma 2 = 10$ nm are the sizes employed in the DC1 along with DC2 when taking into account the 30 nm YIG.

Measurement: Metrics for circuit analysis of performance may be extracted from the compact physical model that is presented to assess how signals travel on each node of the network. The model considers the material parameters such the gyro magnetism ratio, damping, saturate magnetic attraction, and exchangeable stiffness, as well as the physical geometry of directional couplers like the route width. The metrics that follows may be estimated thanks to the model: power use, delayed propagation, and occupied area. The bounding box containing each directional coupler may be employed to calculate the area occupied.

$$ADC = wDC * LDC$$

where wDC stands for the DC's width, which is equal to 2w + 4 • 5 h, where w and h stand for width and its thickness, accordingly [6]. The minimal distance required for two wave guides to have minimal dipolar interaction is calculated using the physical geometryrelated parameter 5 h. The actual length of the coupler is denoted by the number LDC, which may be calculated as $Lw + 2.5 hsin\phi$, where ϕ is the angle of the waveguide's opening or closing arms. The same methodology is used to determine the outer limits of the regenerators and, thus, calculating the network's total area. By dividing the total length of each block by the spin waves subgroup the speed, one can determine the input-output delay generated by each element. Since the ensemble's velocity depends on the wave number, the model considers the three regions' contributions. The propagation delay is modelled in regions 1 and 3 as being reliant on the spin wave passing in an isolated wavelength (k0). Sector 2, on the other hand, considers how the two modalities with differing delays propagate. Generally speaking, τzonei= Lzonei/vgri may be used to calculate the allocation from each zone. All the factors that contributed are added up, considering the biggest delay caused by area 2 (the worst-case scenario), to determine the total calculation time of a single device:

$$\tau_{DC} = \tau_{zone_1} + \max\{\tau_{zone_2}^s, \tau_{zone_2}^{as}\} + \tau_{zone_3}$$

This method is used for all unidirectional couplers. For instance, two directional couplers (DC1 and DC2) and two regenerator blocks—one for the output S and one for the output C-make up the HA discussed in this study. Due to their differing lengths, the two regenerators cause two distinct delays:

$$\begin{split} \tau_{HA_S} &= \tau_{DC_1} + \tau_{DC_2} + \tau_{reg_S} \\ \tau_{HA_C} &= \tau_{DC_1} + \tau_{DC_2} + \tau_{reg_C} \end{split}$$

In this early model versions, the delays caused by both the phase shifter and amplifier are regarded as insignificant. Up to the output, the calculated delay is then passed on to the next computational components. The total of the VCMA amplification (Eamp) and spin wave excitation (ESW) is used to compute the amount of energy required. According to [6], both the energy



DATA SCIENCE AND IOT MANAGEMENT SYSTEM

ISSN: 3068-272X www.ijdim.com Original Research Paper

needed to motivate the spin a wave and the one that powers the energy needed by the amplification was determined to be 12.3 aJ and 3 aJ per the flight, correspondingly.

For Co Fe Bultra-thin films having noticeable VCMA productivity, the estimations are carried out quantitatively. Despite notable advancements in their creation, audio amplifiers with the necessary characteristics are yet to be achieved. The 100nm node is referenced by these numbers. The energy needed to trigger the spin wave drops to 1.96aJ when the technology is scaled to 30 nm. There is no spin wave excitation or power dissipation when logic "0" is present at the circuit input. Consequently, the likelihood that the input will adopt logic "1" (stimulated spin wave) determines the power usage.

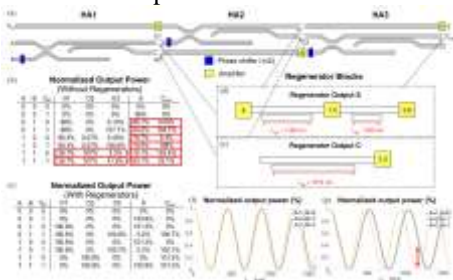
We considered an input chance for neatness, which is $P(A =_ 1_) = P(B =_ 1_) = 0.5$ for the HA. The following formula may be used to determine the electricity utilization:

$$E_{HA} = P(A = {}^{t}1') \cdot E_{SW_A} + P(B = {}^{t}1') \cdot E_{SW_B} + \sum_{i}^{S} E_{amp_j}^{HA}$$

wherein the increased spin wave energies for inputs A and B are denoted by ESWA and ESWB, accordingly. The impact of the S amps, which include regenerators, needed by the HA is considered in the final summation. The HA is a fundamental component used to build more intricate circuits. Consequently, it is simple to generalize equation (21) to various components with inputs of N and M HA as follows:

$$E_{HA} = \sum_{i}^{N} +P_{i}(i = 1') \cdot E_{SW_{i}} + \sum_{j}^{M} E_{amp_{j}}^{HA}$$

wherein ESWi is the ESW of the ith input, assuming logic "1" with an expected value Pi.



4. SIMULATION RESULTS:

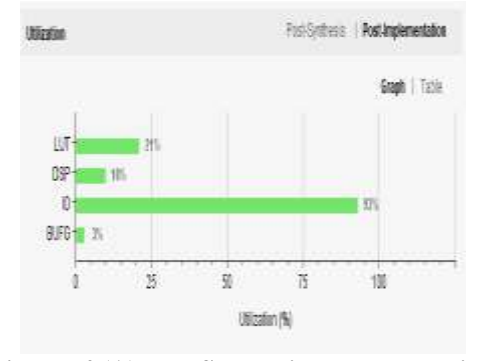


Figure: 4 (A) Post Synthesis Implementation



Figure :4 (B) Power Analysis on Chip Design

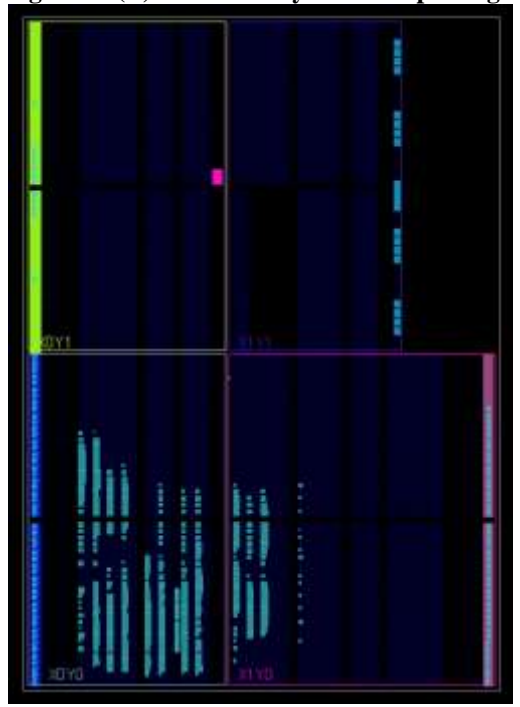


Figure: 4 (C) Elaborating Synthesize Design



Figure: 4 (D) Simulation Behaviour of Design



DATA SCIENCE AND IOT MANAGEMENT SYSTEM

ISSN: 3068-272X www.ijdim.com Original Research Paper

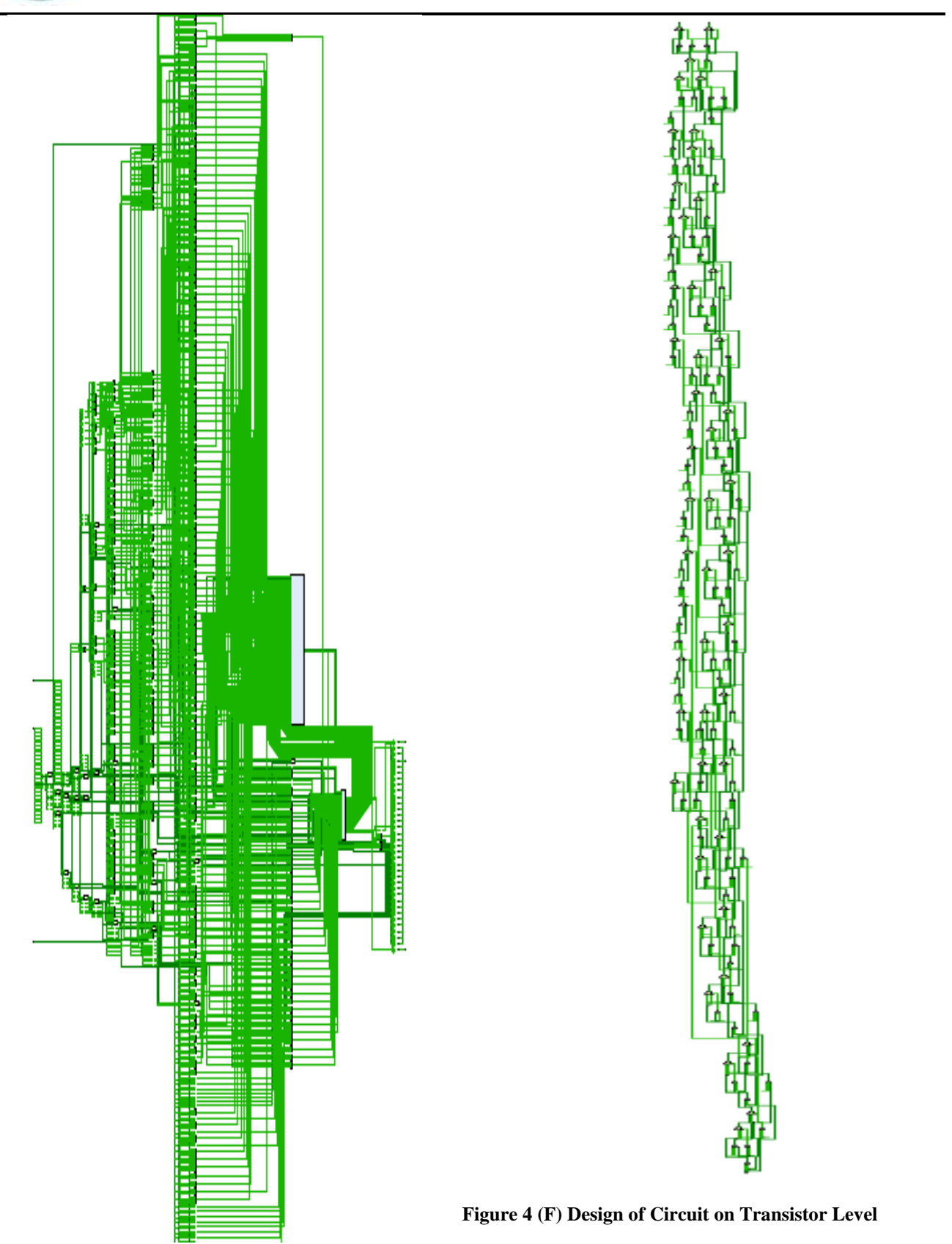


Figure: 4 (E) Design of Circuit on Gate Level



DATA SCIENCE AND IOT MANAGEMENT SYSTEM

ISSN: 3068-272X www.ijdim.com Original Research Paper

5. CONCLUSION

It is feasible to see that not much work has been done to build a technique to examine this potential technology at the circuit level when comparing the studies that have been published on spin wave logic devices. The goal of this effort was to create a small model that can be downloaded here and made publicly available to researchers everywhere. This model would help bridge the gap between building professionals and technologists by allowing for the replication of huge all-magnon circuits. Designing -based systems based on the 100 nm and 30 nm YIG technological advances nodes is made possible by the model. Additionally, the 32-bit rippling carry addition has been taken into consideration as an example to confirm that the model is accurate. The investigation made clear that regenerators are necessary to recover the signal value prior to feeding the subsequent computational element. Furthermore, it is possible to extract circuits metrics such as area work, as latency, and wasted energy. All-magnon systems and cutting-edge spintronic technological advances, such as the FA design suggested in, might be compared using the suggested technique. To guide future research on s, even at the circuit level, we believe that this conceptual framework will be useful. Metrics derived from the model that was given showed that additional work must be done to optimize the spin waves or use different approaches. It would be intriguing to include the connected circular ring element and the orderly circuit notion for rotation wave determining in a future study. Additionally, designers of circuits would be able to readily explore new customized computing components that are now not part of the set of computational parts with the use of a specialized GUI that interacts with the model. Of course, there are still technical issues that need to be resolved, such as the actual assembly of a VCMA booster, which is essential to regenerator design.

REFERENCES

- [1] R. Hertel, W. Wulfhekel, and J. Kirschner, "Domain-wall induced phase shifts in spin waves," Phys. Rev. Lett., vol. 93, 2004, Art. no. 257202.
- [2] P. Pirro, V. I. Vasyuchka, A. A. Serga, and B. Hillebrands, "Advances in coherent magnonics," Nature Rev. Mater., vol. 6, pp. 1114-1135, 2021.
- [3] T. Ichimura, R. Nakane, G. Tanaka, and A. Hirose, "A numerical exploration of signal detector arrangement in a spin-wave reservoir computing device," IEEE Access, vol. 9, pp. 72637-72646, 2021. [4] Á. Papp, G. Csaba, and W. Porod, "Opticallyinspired computing based on spin waves," in Proc. IEEE Int. Conf. Rebooting Comput., 2016, pp. 1–4.
- [5] M. Krawczyk and D. Grundler, "Review and prospects of magnonic crystals and devices with reprogrammable band structure," J. Phys. Condens. Matter, vol. 26, no. 12, 3 2014, Art. no. 123202.

- [6] Q. Wang et al., "A magnonic directional coupler integrated magnonic half-adders," Nature Electron., vol. 3, no. 12, pp. 765-774, 2020.
- [7] A. Mahmoud, F. Vanderveken, F. Ciubotaru, C. Adelmann, S. Hamdioui, and S. Cotofana, "Spin wave based approximate computing," IEEE Trans. Emerg. Topics Comput., vol. 10, no. 4, pp. 1932–1940, Fourth Ouarter 2021.
- [8] Y. Kajiwara et al., "Transmission of electrical signals by spin-wave interconversion in a magnetic insulator," Nature, vol. 464, no. 7286, pp. 262-266,
- [9] M. Collet et al., "Spin-wave propagation in ultrathin YIG based waveguides," Appl. Phys. Lett., vol. 110, no. 9, 2017, Art. no. 092408.
- [10] H. Oin, R. B. Holländer, L. Flajšman, and S. van Dijken, "Low-loss nanoscopic spin-wave guiding in continuous yttrium iron garnet films," Nano Lett., vol. 22, pp. 5294–5300, 2022.
- [11] C. Liu et al., "Long-distance propagation of short-wavelength spinwaves," Nature Commun., vol. 9, 2018, Art. no. 738.
- [12] T. Goto et al., "Three port logic gate using forward volume spin wave interference in a thin yttrium iron garnet film," Sci. Rep., vol. 9, no. 1-11, 2019, Art. no. 16472.
- Talmelli et al., "Reconfigurable [13] G. submicrometer spin-wavemajority gate with electrical transducers," Sci. Adv., vol. 6, 2020, Art. no. eabb4042.
- [14] S. Wintz et al., "Magnetic vortex cores as tunable spin-wave emitters," Nature Nanotechnol., vol. 11, no. 11, pp. 948–953, 2016.
- [15] P. Che, K. Baumgaertl, A. Kúkol'ová, C. Dubs, and D. Grundler, "Efficient wavelength conversion of exchange magnons below 100 nm by magnetic coplanar waveguides," Nature Commun., vol. 11, no. 1, 2020, Art. no. 1445.
- [16] P. Krivosik and C. E. Patton, "Hamiltonian formulation of nonlinear spin wave dynamics: Theory and applications," Phys. Rev. B, vol. 82, 2010, Art. no. 184428.
- [17] R. Verba, V. Tiberkevich, and A. Slavin, "Hamiltonian formalism for nonlinear spin wave dynamics under antisymmetric interactions: Application to Dzyaloshinskii-Moriya interaction," Phys. Rev. B, vol. 99, 2019, Art. no. 174431.
- [18] T. Brächer and P. Pirro, "An analog magnon adder for all-magnonic neurons," J. Appl. Phys., vol. 124, no. 15, 2018, Art. no. 152119.
- [19] G. Csaba, Á. Papp, and W. Porod, "Perspectives of using spin waves for computing and signal processing," Phys. Lett. A, vol. 381, no. 17, pp. 1471-1476, 2017.
- [20] A. Mahmoud et al., "Introduction to spin wave computing," J. Appl. Phys., vol. 128, no. 16, 2020, Art. no. 161101.



DATA SCIENCE AND IOT MANAGEMENT SYSTEM

ISSN: 3068-272X www.ijdim.com Original Research Paper

- [21] A. V. Chumak et al., "Advances in magnetics roadmap on spin-wave computing," IEEE Trans. Magn., vol. 58, no. 6, pp. 1-72, Jun. 2022.
- [22] Q. Wang, A. Chumak, and P. Pirro, "Inversedesign magnonic devices," Nature Commun., vol. 12, no. 1, pp. 1–9, 2021.
- [23] A. Papp, W. Porod, and G. Csaba, "Nanoscale neural network using non-linear spin-wave interference," Nature Commun., vol. 12, 2021, Art. no. 6422.
- [24] K.-S. Lee and S.-K. Kim, "Conceptual design of spin wave logic gates based on a Mach-Zehnder-type spin wave interferometer for universal logic functions," J. Appl. Phys., vol. 104, no. 5, 2008, Art. no. 053909.
- [25] T. Schneider, A. A. Serga, B. Leven, B. Hillebrands, R. L. Stamps, and M. P. Kostylev, "Realization of spin-wave logic gates," Appl. Phys. Lett., vol. 92, no. 2, 2008, Art. no. 022505.
- [26] A. V. Chumak, A. A. Serga, and B. Hillebrands, "Magnon transistor for all-magnon data processing," Nature Commun., vol. 5, no. 1, 8 2014, Art. no. 4700.
- [27] H. Wu et al., "Magnon valve effect between two magnetic insulators," Phys. Rev. Lett., vol. 120, 2018, Art. no. 097205.
- [28] S. Dutta et al., "Non-volatile clocked spin wave interconnect for beyond-CMOS nanomagnet pipelines," Sci. Rep., vol. 5, no. 1, 2015, Art. no.
- [29] E. Egel, C. Meier, G. Csaba, and S. Breitkreutzvon Gamm, "Design of a cmos integrated on-chip oscilloscope for spin wave characterization," AIP Adv., vol. 7, no. 5, 2017, Art. no. 056016.
- [30] A. Mahmoud, F. Vanderveken, C. Adelmann, F. Ciubotaru, S. Hamdioui, and S. Cotofana, "Fan-out enabled spin wave majority gate," AIP Adv., vol. 10, no. 3, 2020, Art. no. 035119.
- [31] A. N. Mahmoud, F.Vanderveken, C.Adelmann, F. Ciubotaru, S. Cotofana, and S.Hamdioui, "Spinwave normalization toward all magnonic circuits," IEEE Trans. Circuits Syst. I: Regular Papers, vol. 68, no. 1, pp. 536-549, Jan. 2021.
- [32] A. V. Sadovnikov et al., "Nonlinear spin wave coupling in adjacent magnonic crystals," Appl. Phys. Lett., vol. 109, no. 4, 2016, Art. no. 042407.
- [33] Q. Wang, P. Pirro, R. Verba, A. Slavin, B. Hillebrands, and A. V. Chumak, "Reconfigurable nanoscale spin-wave directional coupler," Sci. Adv., vol. 4, no. 1, 2018, Art. no. e1701517.
- [34] A. V. Sadovnikov, S. A. Odintsov, E. N. Beginin, S. E. Sheshukova, Y. P. Sharaevskii, and S. A. Nikitov, "Toward nonlinear magnonics: Intensitydependent spin-wave switching in insulating sidecoupled magnetic stripes," Phys. Rev. B, vol. 96, 2017, Art. no. 144428.
- [35] K.Y. Guslienko and A.N. Slavin, "Boundary formagnetization conditions in magnetic nanoelements," Phys. Rev. B, vol. 72, 2005, Art. no. 014463.

- [36] R.Verba, G. Melkov, V. Tiberkevich, and A. Slavin, "Collective spin-wave excitations in a twodimensional array of coupled magnetic nanodots," Phys. Rev. B, vol. 85, 2012, Art. no. 014427.
- [37] R. Verba, M. Carpentieri, G. Finocchio, V. Tiberkevich, and A. Slavin, "Excitation of propagating spin waves in ferromagnetic nanowires magnetic microwave voltage-controlled anisotropy," Sci. Rep., vol. 6, no. 1, 2016, Art. no. 25018.
- [38] B. Heinz et al., "Propagation of spin-wave packets in individual nanosized yttrium iron garnet magnonic conduits," Nano Lett., vol. 20, no. 6, pp. 4220-4227, 2020.
- [39] M. Beleggia, S. Tandon, Y. Zhu, and M. De Graef, "On the magnetostatic interactions between nanoparticles of arbitrary shape," J. Magnetism Magn. Mater., vol. 278, no. 1, pp. 270-284, 2004.
- [40] Y.-J. Chen et al., "Parametric resonance of magnetization excited by electric field," Nano Lett., vol. 17, no. 1, pp. 572–577, 2017.
- [41] O. V. Dobrovolskiy et al., "Spin-wave phase inverter upon a single nanodefect," ACS Appl. Mater. Interfaces, vol. 11, no. 19, pp. 17654–17662, 2019.
- [42] Y. Au, M. Dvornik, O. Dmytriiev, and V. V. Kruglyak, "Nanoscale spin wave valve and phase shifter," Appl. Phys. Lett., vol. 100, no. 17, 2012, Art. no. 172408.